Experimental Cell Research **275,** 230–242 (2002)
doi:10.1006/excr.2002.5481, available online at http://www.idealibrary.com on IDEAL®

Macrophages Influence a Competition of Contact Guidance and Chemotaxis for Fibroblast Alignment in a Fibrin Gel Coculture Assay

B. A. Bromberek,* P. A. J. Enever,* D. I. Shreiber,* M. D. Caldwell,†,[1] and R. T. Tranquillo*,‡,[2]

**Department of Chemical Engineering & Materials Science, ‡Department of Biomedical Engineering, and †Department of Surgery, University of Minnesota, Minneapolis, Minnesota 55455*

Rat dermal fibroblasts were dispersed initially in the outer shell of a fibrin gel sphere, while the inner core either was devoid of cells or contained peritoneal exudate cells (primarily macrophages), thereby mimicking the inflammatory phase of wound healing. The fibroblasts compacted floating fibrin microspheres over time. In the absence of macrophages, the initial distribution of fibroblasts (only in the shell) induced circumferential alignment of fibrin fibrils via compaction of the shell relative to the core. The aligned fibrils created a contact guidance field, which was manifested by strong circumferential alignment of the fibroblasts. However, in the presence of macrophages, the fibroblasts exhibited more radial alignment despite the simultaneous contact guidance field in the circumferential direction associated with compaction. This was attributed to a chemotactic gradient emanating from the core due to a putative factor(s) released by the macrophages. The presence of a radial chemotactic stimulus was supported by the finding of even greater radial alignment when fibrin microspheres were embedded in an agarose–fibrin gel that abolished compaction and consequently the contact guidance field. Our assay permits the simulation of tissue morphogenetic processes that involve cell guidance phenomena and tractional restructuring of the extracellular matrix.

Key Words: **coculture assay; wound healing; fibroblasts; macrophages; fibrin gel; contact guidance; chemotaxis.**

INTRODUCTION

A number of important biological phenomena involve the interplay between cellular traction and directed migration. Chief among them are mesenchymal morphogenetic processes such as tumor stroma formation [1], embryogenesis [2], teratoma formation [3], and wound contraction [4] in which directed migration both affects and is affected by tractional restructuring of the extracellular matrix (ECM) through a complex feedback mechanism [5]. Cell migration may be directed by spatial gradients of soluble factors (i.e., chemotaxis) and/or fibril alignment within the ECM (i.e., contact guidance). The resulting inhomogeneous distribution of cells gives rise to inhomogeneous deformation of the ECM that may generate or reinforce contact guidance fields [6]. This affects the subsequent ECM restructuring, which ultimately determines the form and structure of the tissue.

The complexity of these biochemical and biomechanical phenomena motivates *in vitro* assays that allow the interplay to be quantitatively manipulated and characterized. Several assays have been employed to study fibroblast chemotaxis [7, 8] or contact guidance [9–11], but they typically involve 2-D substrata of minimal biological relevance. In contrast, the fibroblast-populated collagen lattice (FPCL) assay proposed by Bell *et al.* [12] and its variants have, through the use of a 3-D biologically relevant substratum, revealed extensive information about tissue contraction and remodeling but not the roles of contact guidance and chemotaxis in tissue formation (e.g., [13–16]). Herein we present a new assay that allows for the study of simultaneous contact guidance and chemotaxis in an environment undergoing tissue contraction and restructuring. Our chosen area of inquiry is wound healing, but the assay could be applied to study a variety of mesenchymal morphogenetic processes.

We have previously developed a spherical analog of the FPCL that we refer to as the fibroblast-populated microsphere (FPM)[3] [17]. The spherical geometry is preferred because it facilitates modeling with our biphasic theory for cell–matrix mechanical interactions that allows us to estimate the traction exerted by the fibroblasts from FPM compaction [18]. Here we introduce a variant of the FPM which we shall designate the

[1] Current address: Marshfield Medical Research Foundation, Marshfield, WI 54449.

[2] To whom correspondence and reprint requests should be addressed. Fax: (612) 626-7246. E-mail: tranquillo@cems.umn.edu.

[3] Abbreviations used: FPCM, fibroblast-populated concentric microsphere; FPM, fibroblast-populated microsphere; RDF, rat dermal fibroblast; PEC, peritoneal exudate cell; US-M199, unsupplemented M199.

0014-4827/02 $35.00

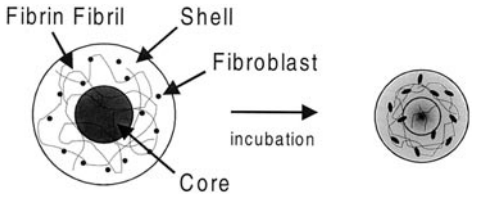

FIG. 1. Schematic of the fibroblast-populated concentric microsphere (FPCM) fibrin gel coculture assay. Initial state of the FPCM (left) and a subsequent state (right) following incubation. Filled ellipses represent fibroblasts and shading depicts the concentration of a diffusible stimulatory factor. A microsphere of fibrin gel is formed that initially has a core devoid of fibroblasts, but which contains a diffusible stimulatory factor in controlled-release form, and an outer concentric shell containing fibroblasts dispersed uniformly. Compaction of the FPCM is measured over time.

fibroblast-populated concentric microsphere (FPCM). The FPCM is composed of two distinct regions as shown in Fig. 1: a core and a concentric shell. Fibroblasts, initially seeded only in the shell, alter their orientation and migration in response to a gradient of a chemotactic factor directed radially outward from the core into the surrounding shell. This configuration mimics that of a wound in which fibroblasts migrate from adjacent unwounded tissue into the fibrin provisional matrix in response to chemotactic factors released within the wound. As in our FPM assay, fibroblast traction results in compaction of the FPCM, which is easily observed and quantified by a reduction in its diameter. However, the spatially inhomogeneous distribution of the fibroblasts results in an inhomogeneous compaction of the FPCM. Based upon our anisotropic biphasic theory for cell–matrix mechanical interactions, this inhomogeneous compaction should result in circumferential fibril alignment and a corresponding contact guidance field [6], even in the absence of chemotaxis.

The spherical geometry of the FPCM affords important advantages over analogous linear and cylindrical geometry configurations and other assays aiming to simulate dermal wound healing and other morphogenetic processes. First, variables are dependent only on the radial dimension because of the spherical symmetry. Second, unlike an analogous assay of cylindrical or "disk" geometry in which the factor can diffuse into the medium and back into the gel at a distant point, the FPCM geometry creates a strict diffusion gradient of the chemotactic factor emanating from the core through the FPCM shell as illustrated in Fig. 2. While the former can be considered only as a convenience advantage in terms of simplifying the characterization, the latter is a crucial advantage because it allows the concentration gradient of the chemotactic factor to be maintained, controlled, and, thereby, predicted. Although not necessarily unique to our assay, another advantage of our approach is minimized gradients of nutrients and metabolites in the gel because of the millimeter scale of the FPCMs we fabricate.

Here we describe the protocol for our FPCM wound assay, investigate the outcome in various configurations in addition to the base case of a fibroblast-seeded shell and an acellular core, and present results for a fibroblast-seeded shell with resident immune cells (peritoneal exudate cells or PEC) dispersed in the core to serve as the source of chemotactic factors. In the absence of PECs in the core, we report a significant circumferential alignment of the fibroblasts that is not seen in the FPM assay, which we attribute to a contact guidance response. We also report an apparent chemotactic response of the fibroblasts to factors generated by the PECs manifested as a change from circumferential alignment to radial alignment, particularly when FPCM compaction is abolished by embedding the FPCM in an agarose–fibrin gel to which it adheres during incubation. A decrease in FPCM compaction in the presence of PECs implies that the change toward radial alignment is also facilitated by a weaker contact guidance response around the circumference.

MATERIALS AND METHODS

Materials

Trypsin (25 mg/ml in 0.9% saline), ethylenediaminetetraacetic acid (EDTA), $CaCl_2$, NaOH, bovine fibrinogen, bovine thrombin, silicone oil, lysine-4B agarose, gelatin-beaded agarose, and low-melting agarose were purchased from Sigma Chemical Co. (St. Louis, MO). Tissue culture medium, penicillin/streptomycin (pen–strep), Fungizone, Hepes buffer, phosphate-buffered saline (PBS), and L-

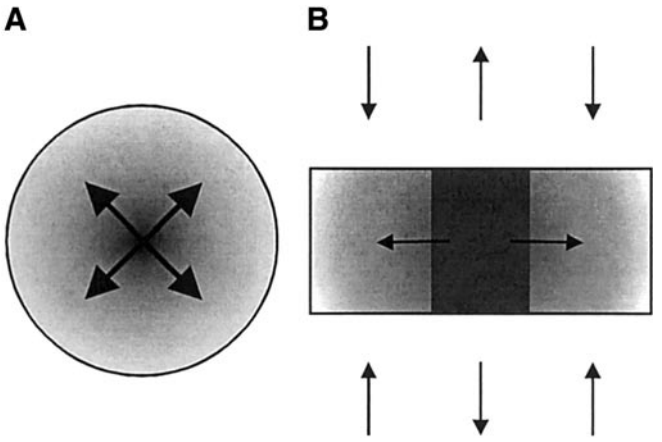

FIG. 2. Diffusion profile of a stimulatory factor diffusing from the core of (A) a spherical fibrin gel and (B) a cylindrical fibrin gel. The spherical geometry creates a strict diffusion gradient in the radial direction. In the cylindrical "disk" geometry, the diffusible factor can diffuse from the core into the medium and then back into the gel at a distant point (e.g., the shell). As a result, the concentration gradient is not based purely on diffusion through the gel, so it cannot be readily maintained, controlled, or predicted in the cylindrical geometry.

glutamine were from Gibco Laboratories (Grand Island, NY). Fetal bovine serum (FBS) was from HyClone Laboratories (Logan, UT). Recombinant human transforming growth factor $\beta 1$ ($rhTGF_{\beta 1}$) was purchased from R&D Systems (Minneapolis, MN). Syringe filters (0.2 and 0.45 μm) were purchased from Gelman Sciences (Ann Arbor, MI).

RDF Culture

Rat dermal fibroblasts (RDFs) were obtained using a primary explant technique [19] and kept in liquid nitrogen after slow freezing. Cell lines were initiated for culture by thawing an aliquot of cells and centrifuging at 1000 rpm for 10 min at 4°C. The pellet of cells was resuspended in Dulbecco's modified Eagle's medium (DMEM) supplemented with pen–strep (1% v/v) and L-glutamine (1% v/v). Cells were plated on 60 × 15-mm petri dishes using 5 ml of DMEM with 10% FBS, 1% pen–strep, 1% Fungizone, and 1% L-glutamine and kept in a humidified CO_2 incubator at 37°C. Trypsin/EDTA was used to pass the cells once a week at a 1:4 dilution. Cells were harvested with 0.5% trypsin/EDTA; washed twice with Medium 199 with Hanks' salts (M199) supplemented with 10% FBS, 1% pen–strep, and 1% L-glutamine; and diluted to a standard concentration of 2×10^5 cells/ml. Cells were passed or harvested at 60–90% confluence. All experiments were conducted before the ninth passage, at which point a new culture was initiated from frozen cells.

Isolation of PECs

PECs were acquired via peritoneal lavage [20]. A Fisher rat (Harlan, Indianapolis, IN) was sacrificed by CO_2 asphyxiation, the abdominal skin was removed, and the peritoneal cavity exposed. The peritoneal cavity was injected with 45 ml of harvest medium (M199 with 0.1% BSA, 1% pen–strep). The solution was withdrawn via syringe and placed in a 50-ml polypropylene conical tube, centrifuged, resuspended in harvest medium, counted, and diluted to 6×10^6 cells/ml. PECs were maintained at 28°C for 2 h in a solution of harvest medium supplemented with 1.25 ng/ml $rhTGF_{\beta 1}$ so as to place the macrophages in a repair and recruitment mode as opposed to cytotoxic mode [21, 22]. Fluorescence-activated cell sorting and differential analysis of rat PECs in our lab has shown them typically to comprise 60 to 70% macrophages with the balance being predominantly lymphocytes and neutrophils [23].

Thrombin Preparation

Bovine thrombin (250 units) was suspended in 1 ml sterile water and 9 ml of PBS, passed through a 0.2-μm syringe filter, divided into 0.125-ml aliquots, and stored at −80°C. For assay use, 100 μl of thrombin from frozen aliquots was added to 1 ml of unsupplemented M199 (US-M199; no additives other than Hepes and Hanks' salts) with 15 μl of 2 M $CaCl_2$ and stored on ice. US-M199 was used since we have found that factors present in FBS can decrease the activity of the thrombin solution.

Fibrinogen Preparation

Type IV bovine fibrinogen (5.5 g) was dissolved in 150 ml of 20 mM Hepes-buffered saline at 37°C and then filtered through a 0.2-μm filter (Nalge Nunc, Naperville, IL). Plasminogen and fibronectin were removed via affinity chromatography by passing the solution through lysine-4B and gelatin-beaded agarose columns. Removal of plasminogen and fibronectin was confirmed by SDS–PAGE. Final protein concentration was determined by absorbance at 280 nm. Fibrinogen was stored as 1-ml aliquots at −80°C. For assay use, a 1-ml aliquot was added to sufficient 20 mM Hepes-buffered saline to make a 5 mg/ml solution and then filtered through 0.45- and 0.2-μm syringe filters.

FPM Assay

FPMs were manufactured using an adaptation of a previously reported technique [17]. A 1-cm layer of "heavy" silicone oil (sg 1.1) was placed in the bottom of a 10 × 2 × 5-cm glass well. An approximately 3-cm-thick layer of "light" silicone oil (sg 0.96) was then added to the well. The silicone oils separated into two distinct layers. The glass wells of silicone oil were then placed in a 37°C incubator.

In a well of a 96-well plate, 100 μl of fibrinogen solution, 25 μl of thrombin solution, and 25 μl of RDF suspension were mixed together. Standard final concentrations in the gel-forming solution were RDFs at 3.33×10^4 cells/ml, thrombin at 0.038 units/ml, and fibrinogen at 3.33 mg/ml. An 80-μl aliquot of the RDF–thrombin–fibrinogen solution was then immediately pipetted into the glass well containing the 37°C silicone oils. The pipette tip was placed just below the surface of the light oil, the contents slowly ejected, and the tip quickly withdrawn. Care was taken to avoid introducing air bubbles into the forming FPM. The FPM slowly settled to the interface between the two silicone oils and retained its spherical shape. FPMs were incubated in the 37°C silicone oil for 15 min to permit fibrin gelation. The resulting FPMs were approximately 5.2 mm in diameter.

FPMs were removed, washed thoroughly with US-M199, and then incubated in complete medium (M199, 10% FBS, 1% pen–strep, 1% L-glutamine, and 1% Fungizone). Remaining silicone oil could occasionally be seen as small (<100 μm diameter) droplets on the FPM surface. The FPMs were then transferred to a new 24-well plate with complete medium for incubation at 37°C for the duration of the experiment.

FPCM Assay

The fabrication of the FPCMs is similar to that of the FPMs except that it is a two-part process as shown in Fig. 3. First, a small fibrin sphere is created, which will form the core of the FPCM. Second, a fibrin gel shell is cast around the core. The distinct core and shell regions of the FPCM make it possible to have spatially varying cell concentrations of one or more cell types. The fabrication methods for five different configurations ("Base," "Control," "Inverse," "Embedded," and "Core stimulus" FPCMs) are detailed below.

Base FPCM assay. The Base FPCM consists of a fibroblast-seeded shell and an acellular core as shown schematically in Fig. 4A. Twenty microliters of fibrinogen solution was mixed with 5 μl of thrombin solution and 5 μl of US-M199, and a 15-μl aliquot of this thrombin–fibrinogen solution was then immediately pipetted into a well containing the layered silicone oils. The FPCM core settled to the interface, retaining its spherical shape, and was incubated in the 37°C oils for 10 min to allow for gelation.

One hundred microliters of the fibrinogen solution was mixed with 25 μl of the thrombin solution and 25 μl of the RDF suspension. A 65-μl aliquot of this RDF–thrombin–fibrinogen solution was pipetted next to a core in the silicone oil to form the shell of the Base FPCM. A 0.05-mm-diameter glass rod, prewetted in US-M199, was used to draw the core into the gelling shell solution. A 22-gauge copper wire loop, connected to the negative terminal of a 1000-V power supply, was used to position the core in the center of the Base FPCM via electrostatic repulsion. The Base FPCMs were incubated in the 37°C silicone oil for 15 min, then removed, washed with US-M199, transferred to a 24-well plate with complete medium, and incubated in air at 37°C for the course of the experiment. The initial FPCM diameter was approximately 5.2 mm, with the initial core diameter being approximately 2.9 mm.

Control FPCM. The Control FPCM is identical to the Base FPCM except that both the core and the shell contain RDFs as indicated in Fig. 4B. This was accomplished by mixing 20 μl of fibrinogen solution with 5 μl of thrombin solution and 5 μl of RDF suspension to form the solution that was used to create the core. The rest of the fabrication procedure was as detailed for the Base FPCM.

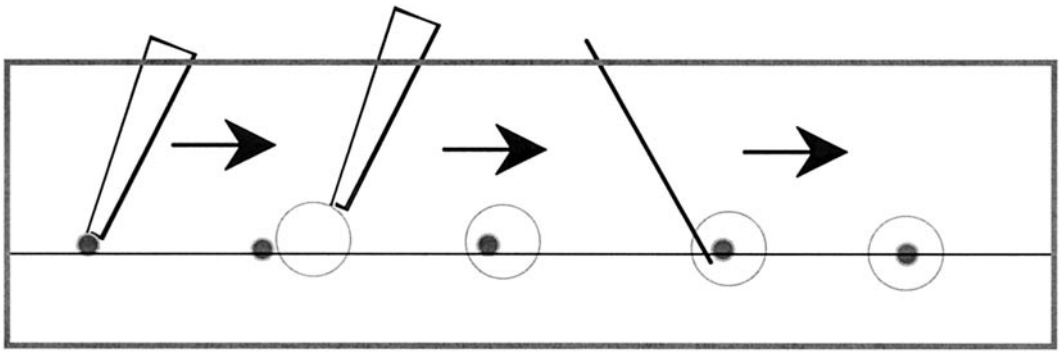

FIG. 3. Schematic of the FPCM manufacture technique. Initially, a fibrinogen–thrombin solution is pipetted into a well containing two silicone oils of differing densities. This core-forming solution settles to the interface between the two silicone oils and takes on a spherical shape because of the surface tension between the silicone oil and the fibrinogen–thrombin solution. A fibrinogen–thrombin–RDF solution is then pipetted next to the core to create the shell, and the core is placed within the shell with a thin glass rod. The core is positioned concentrically within the shell with a negatively charged copper loop via electrostatic repulsion (not shown).

Inverse FPCM. The Inverse FPCM has a fibroblast distribution that is the inverse of that of the 'Base' FPCM; RDFs are seeded in the core but not in the shell as shown in Fig. 4C. The core was formed from a solution prepared by mixing 20 μl of fibrinogen solution with 5 μl of thrombin solution and 5 μl of RDF suspension. The shell was formed from a solution created by mixing 100 μl of fibrinogen solution with 25 μl of thrombin solution and 25 μl of US-M199. The fabrication technique was otherwise identical to that of the Base FPCM.

Embedded FPCM. FPCMs were prepared as detailed above. As an alternative to allowing them to float and compact freely during incubation, an embedding method was devised to prevent compaction as shown schematically in Fig. 4D. A solution of 1.0% low-melting agarose and 0.5 mg/ml fibrinogen in complete medium was prepared. A 350-μl aliquot of the embedding solution was pipetted into a Millicell plate insert (Millipore, Bedford, MA). A prepared FPCM was positioned in the Millicell, and 5 μl of thrombin was added. The Embedded FPCM was incubated at 37°C for 20 min until fibrin gelation was complete, then placed in a cold room (4°C) for 1 h until agarose gelation was complete. The Millicell inserts were placed in the wells of a 24-well plate with 1.5 ml of complete medium and incubated at 37°C for the duration of the experiment.

Core stimulus FPCMs. As indicated in Fig. 4E, distributed sources of chemotactic factors, in these studies PECs, were seeded in the core of the FPCM, with RDFs seeded in the shell. The fabrication technique was identical to that of the Base FPCM except that 20 μl of fibrinogen solution was mixed with 5 μl of thrombin solution and 5 μl of PEC suspension (at 6× the desired final PEC concentration) to create the FPCM core solution.

FPM and FPCM Analysis

A 24-well plate containing FPMs or FPCMs was placed on the stage of an Olympus IX-70 inverted light microscope (Melville, NY). Images of the equatorial plane of each microsphere were captured with a Photometrics SenSys cooled CCD camera (Tucson, AZ) using a 4× objective. A motorized microscope stage was used to capture a series of images to form a mosaic of the entire FPM or FPCM.

Diameter measurement. Diameter measurements were made immediately after FPM or FPCM preparation and at subsequent time points. To accomplish this, the mosaic image of the microsphere was modified in an image manipulation program. White dots were used to mark the surface; smaller dots were also placed around the core for FPCMs. The images were analyzed with image analysis software (Inovision, Raleigh, NC) and the positions of the dots were reported. The diameter and center of the FPM or the FPCM shell and core were estimated by fitting the data via least-squares regression to the equation for a circle, yielding the diameters and centers of the best-fit circles. The degree of compaction, ρ, was calculated as the percentage decrease of diameter with respect to its initial value.

Measurement of FPCM concentricity. Concentricity, χ, of the core of a FPCM with respect to the shell was determined from the initial time point image according to

$$\chi = 1 - \frac{\sqrt{\Delta x^2 + \Delta y^2 + \Delta z^2}}{R_{\text{shell}} - R_{\text{core}}},$$

where χ ranged from 0 (core touching the FPCM surface) to 1 (concentric). The values of Δx and Δy were calculated from the difference in location between the core and the shell centers as determined from the diameter measurements. The value of Δz was determined by recording the difference in z position between the plane of focus for the FPCM shell equatorial plane and that of the core.

Measurement of RDF alignment. The RDF alignment with respect to a radial vector emanating from the center of the FPM or FPCM was described by the parameter Φ, ranging from 0 for circumferential alignment to 1 for radial alignment. Φ was defined as $\cos^2(\alpha)$ where α was the angle made by the major axis of the cell and the radial vector passing though the cell centroid as shown in Fig. 5. A Φ value for each elongated, in-focus cell in the microsphere image mosaic was determined as follows. The major axis of a cell was marked with a line in an image manipulation program and feature information was extracted using image analysis software. Using the cell length, cell centroid position, and FPM center or FPCM core center position, α and Φ were calculated. Φ values for all marked cells were averaged to obtain the mean cell alignment for a microsphere, $<\Phi>$. Values for n replicate microspheres in a group were averaged to calculate $<\Phi>_n$, the mean for the group.

Statistical testing. Comparisons between $<\Phi>_n$ values were performed using either a one-tailed or a two-tailed t test as appropriate. Significance levels were set at $P < 0.05$. The effects of PEC loading concentration and incubation time on cell alignment were analyzed with a two-way analysis of variance (ANOVA) with significance levels set at $P < 0.05$.

Fibril alignment. Direct observation of the alignment of fibrin fibrils in the compacting FPCMs was accomplished using polarized light microscopy. Individual FPCMs were transferred to a chamber possessing a strain-free glass bottom and filled with complete me-

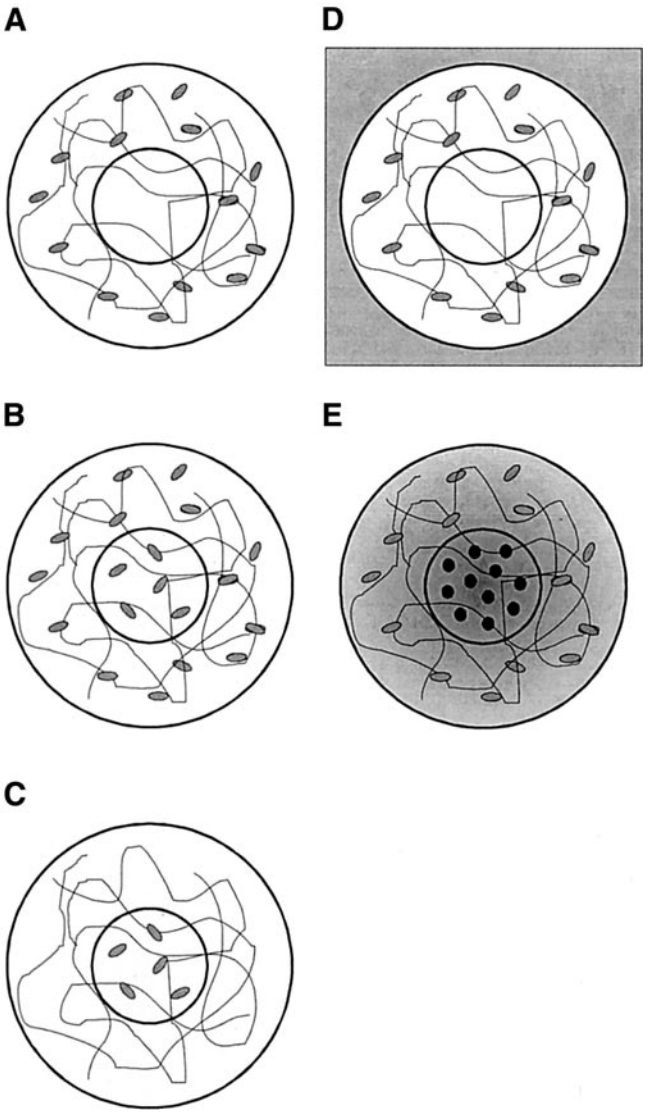

FIG. 4. Schematics of the various FPCM configurations. (A) "Base" FPCM: RDFs in the shell; no cells in the core. (B) "Control" FPCM: RDFs in the core and shell at a uniform concentration. (C) "Inverse" FPCM: RDFs in the core; no cells in the shell. (D) "Embedded" FPCM: FPCM (Base FPCM shown) embedded in an agarose–fibrin gel that restricts compaction. (E) "Core stimulus" FPCM: RDFs in the shell; PECs in the core.

dium. The chamber was placed on a rotating stage and then rotated while viewed under crossed polarizing filters.

RESULTS

FPM Assay

With a uniform distribution of RDFs throughout the fibrin gel, we observed uniform FPM compaction and random cell orientation (Table 1). The behavior observed in the FPM provides a benchmark for assessing results observed in the various FPCM configurations.

FPCM Assay

One of the central assumptions of the FPCM assay is that the core and shell are concentric. Therefore, before considering the results of the FPCM assay, it was necessary to consider the consequences of eccentricity of the core and shell, measured by χ, as perfect concentricity cannot be realized. We manufactured Base FPCMs with χ values ranging from approximately 0.6 to 1.0 and then performed a comparison among all possible pairs of $<\Phi>$ values with Scheffe's post hoc test with a null hypothesis that there is no significant difference between the $<\Phi>$ values for FPCMs of varying χ. At the level of significance of $P < 0.05$, the null hypothesis could not be rejected in any case. This suggests that FPCMs with a χ value of 0.6 or greater yield results that are not significantly affected by the eccentricity. In this study, 90% of the FPCMs scored had a χ value exceeding 0.6.

Strong Circumferential Alignment of RDFs Occurs in Floating FPCMs without PECs in the Core, but Not in Embedded FPCMs

We first investigated Base FPCMs to establish a basis for comparison (unless stated as Embedded, all FPCMs discussed were free-floating). Figure 6A shows an equatorial plane of a Base FPCM immediately after

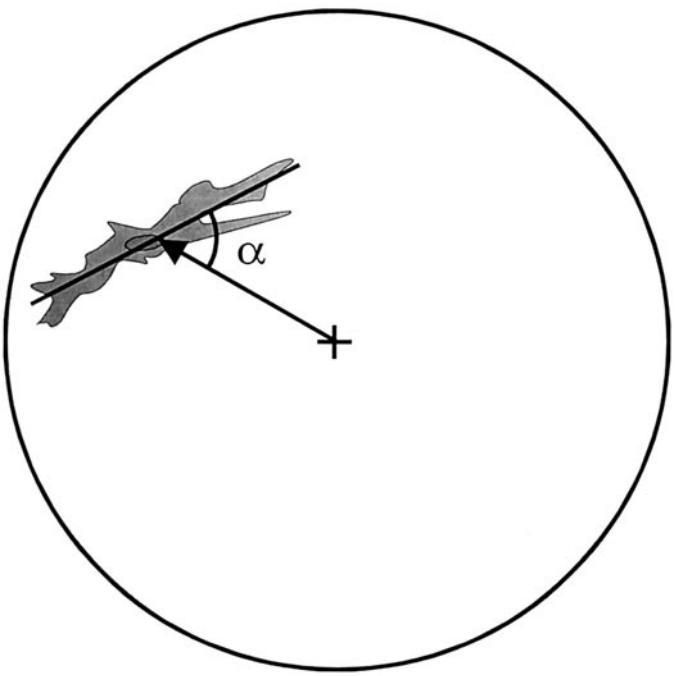

FIG. 5. Method for determining cell alignment angle, α. The long axis of the cell is determined via image analysis software, and the angle between the long axis and the radial vector from the center of the FPM or FPCM is calculated. The alignment parameter, Φ, for a given cell is defined as $\cos^2(\alpha)$.

TABLE 1

FPCMs without PECs in the Core

Assay type	n	$\langle\chi\rangle$	$\langle\rho_{shell}\rangle$ (%)	$\langle\rho_{core}\rangle$ (%)	$\langle\Phi\rangle_n$	σ_Φ	P value
FPM	9	N/A	12	NA	0.48	0.02	0.300
FPCM–Base	12	0.61	20	12	0.25	0.02	<0.001
FPCM–Control	16	0.76	19	17	0.47	0.01	0.082
FPCM–Inverse	10	0.70	24	63	0.95	0.01	<0.001
FPCM–Embedded	8	0.74	0	0	0.51	0.03	0.568

Note. σ_Φ denotes standard error of the mean. Incubation time was 24 h in all cases.

fabrication and Fig. 6B shows it following 24 h of incubation, during which time the FPCM diameter decreased by 21.5%. Figure 7A is a cell alignment plot derived from Fig. 6B based on determination of alignment for in-focus cells and perimeters of the FPCM shell and core. The cell alignments are color-coded to facilitate visualization of the alignment distribution. The value of $\langle\Phi\rangle$ was 0.21, consistent with an obvious circumferential alignment of the cells. Values for replicate samples are summarized in Table 1, showing a difference ($\langle\Phi\rangle_{n=12} = 0.25$) from theoretical random cell orientation ($\langle\Phi\rangle = 0.5$) to be highly significant. Using the biphasic theory for cell–matrix mechanical interactions, we have previously attributed this result to a contact guidance response of the RDFs due to circumferential alignment of the fibrin fibrils induced by compaction of the shell relative to the core because RDFs are initially absent from the core [6]. It is readily seen in Figs. 6B and 7A that the RDFs did not populate the core of the Base FPCM during the incubation period. This led us to investigate other configurations of the assay (Fig. 4).

Control FPCMs were constructed to ascertain whether the observed circumferential RDF alignment in the Base FPCM was an artifact of the FPCM fabrication technique or a result of the nonuniform cell distribution. Our theory for cell–matrix mechanical interactions predicts random orientation if cells are distributed uniformly throughout the FPCM and the fibrin fibrils are initially randomly oriented, as is the case in the FPM, because the FPCM compacts uniformly. The Control FPCM has a uniform cell distribution like that of the FPM. Therefore, any difference in cell alignment between the FPM and Control FPCM would indicate the presence of an artifact which is introduced during the two-step FPCM fabrication technique. As indicated in Fig. 7B, random orientation was observed in the Control FPCM. This is confirmed in Table 1, which shows that $\langle\Phi\rangle_n$ was not significantly different from random orientation ($P = 0.08$); it was also not significantly different from $\langle\Phi\rangle_n$ for FPMs ($P = 0.48$). Hence, we concluded that the two-step FPCM fabrication technique is not the cause of the circumferential cell alignment observed in the Base FPCM. The strong circumferential alignment would help explain the lack of core invasion by the RDFs: cells would tend to migrate around the circumference of the FPCM shell due to contact guidance. Time-lapse microscopy revealed that cell migration was very limited, so that strong circumferential contact guidance could effectively inhibit core invasion.

To ensure that the two-step fabrication method did not create an "interface" that would prevent invasion in the absence of strong circumferential contact guidance and/or with greater cell migration, we fabricated Inverse FPCMs, in which RDFs were initially dispersed in the core but not in the shell. A typical outcome is shown in Fig. 7C. As core compaction occurred, cells migrated outward from the core into the shell, with strong radial alignment (Table 1; $\langle\Phi\rangle_{n=10} = 0.95$). While other explanations are possible (e.g., an "avoidance response" due to the increased cell concentration in the core, presumably via chemotaxis), the theory for cell–matrix mechanical interactions also predicts this as another manifestation of contact guidance [6]. Here, the fibrils in the shell become radially aligned due to the compaction of the core relative to the shell. Polarized light microscopy confirms this explanation. Figure 8A shows a radial birefringence pattern for an Inverse FPCM, indicating radial alignment of fibrin fibrils. In contrast, Fig. 8B shows four bright regions in the shell of a Base FPCM. Though the presence of cells interferes with the birefringence pattern, the four bright regions are consistent with circumferential fibril alignment as is the observation that they rotated as the crossed polarizers were rotated with respect to the FPCM. Furthermore, no such bright regions were observed in either FPMs or Control FPCMs (not shown).

The Inverse FPCMs clearly showed that cells are capable of migration across the core–shell interface. Moreover, there was no evidence of core detachment from the shell in any of these FPCMs, indicating that the interface is structurally continuous. Thus, the Inverse FPCMs demonstrate that any possible artifacts introduced via the fabrication procedure, such as a

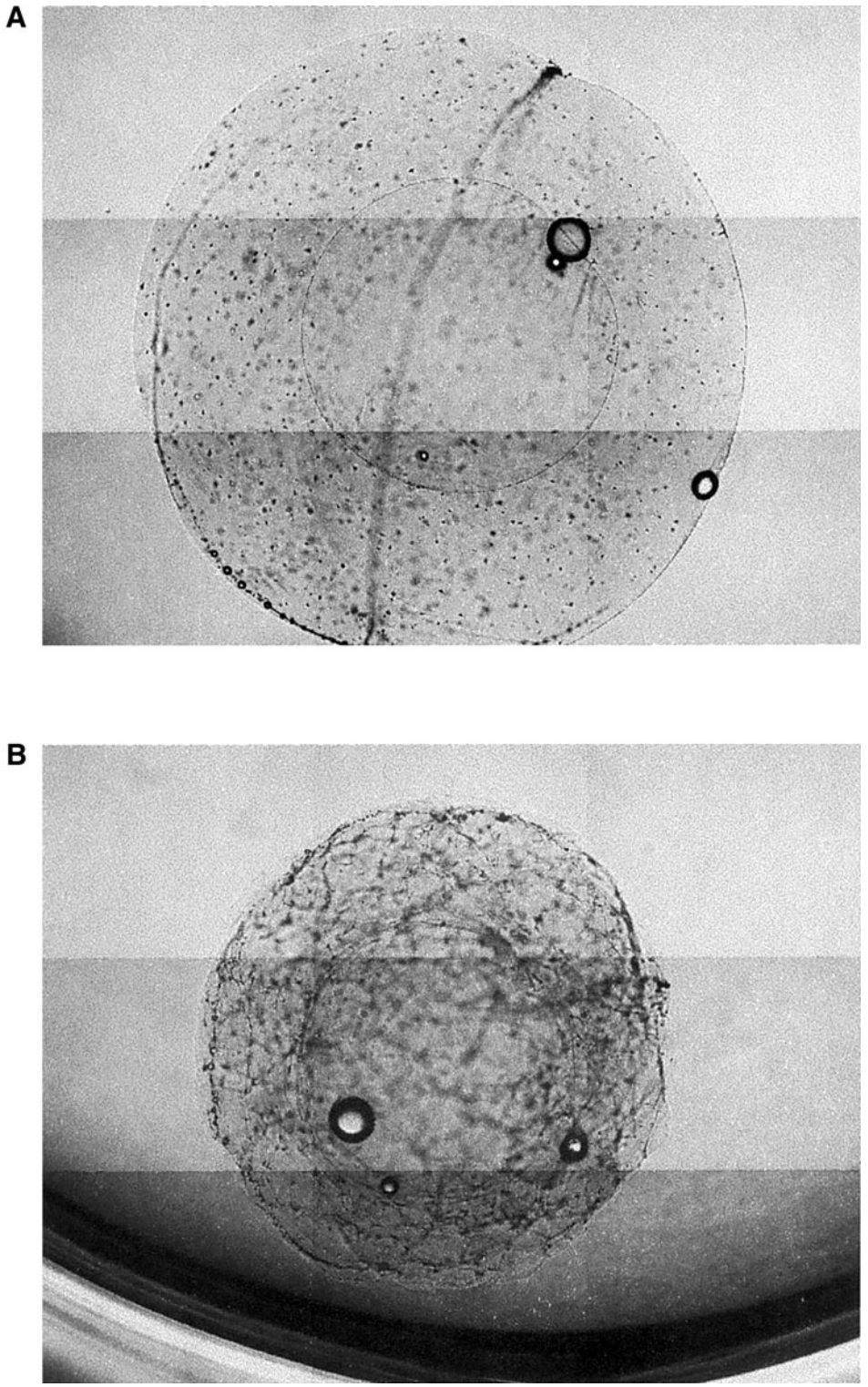

FIG. 6. Digitial light micrographs of a FPCM (A) immediately following fabrication and (B) after 24-h incubation. Several residual droplets of silicone oil are evident on the surface of this FPCM. RDFs appear as small spherical inclusions in the FPCM shell before spreading and FPCM compaction and generally appear elongated after spreading and during the initial compaction period studied. Circumferential alignment of RDFs is evident after the 24-h incubation: ρ_{shell} = 19%, $<\Phi>$ = 0.21, and χ = 0.81 for (B).

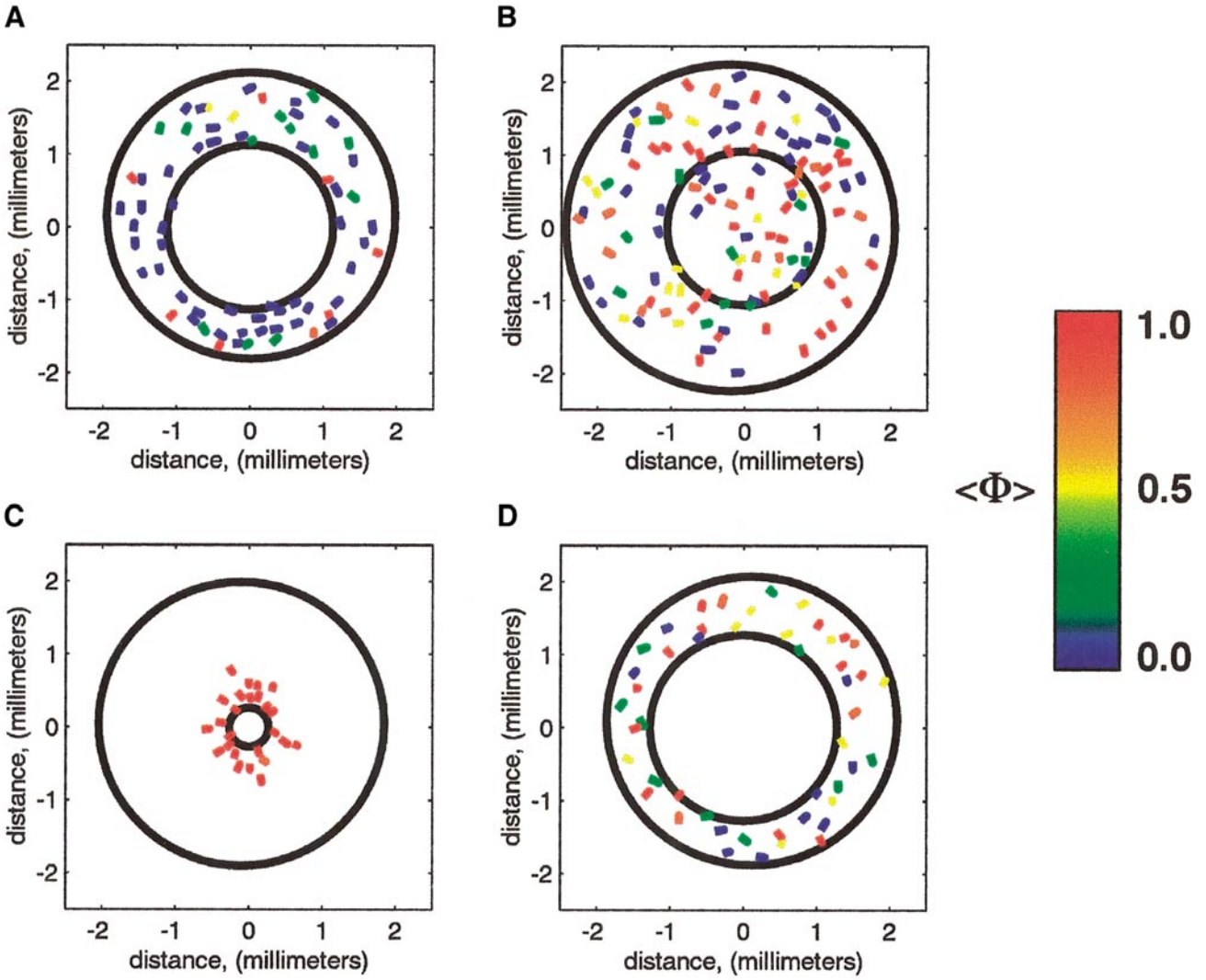

FIG. 7. Cell alignment plots for various FPCMs. Cells are color coded to indicate alignment parameter value. Blue cells are circumferentially aligned ($\Phi < 0.2$) while red cells are radially aligned ($\Phi > 0.8$). (A) Base FPCM (same as in Fig. 6): $\rho_{shell} = 19\%$, $<\Phi> = 0.21$, and $\chi = 0.81$. (B) Control FPCM: $\rho_{shell} = 16\%$, $<\Phi> = 0.51$, and $\chi = 0.84$. (C) Inverse FPCM: $\rho_{shell} = 14\%$, $\rho_{core} = 50\%$, $<\Phi> = 0.94$, and $\chi = 0.96$. (D) Core stimulus FPCM with PECs at 5×10^6 cells/ml dispersed in the core: $\rho_{shell} = 18\%$, $<\Phi> = 0.50$, and $\chi = 0.77$. Incubation period was 24 h for all FPCM schematics except (D), for which the incubation period was 48 h.

local circumferential guidance field along the interface, do not preclude invasion in all circumstances.

Finally, we investigated Base FPCMs embedded in an agarose–fibrin gel, termed Embedded FPCMs (Fig. 4D), which abolished compaction due to strong adhesion of the FPCM to the gel. Without compaction, the initial random orientation of RDFs was sustained (Table 1), in agreement with the cell–matrix mechanical interaction theory prediction that compaction of the shell relative to the core drives circumferential alignment.

Taken collectively, these results support the conclusion that the circumferential alignment observed for Base FPCMs (Figs. 6B and 7A) resulted from a contact guidance response of the RDFs due to circumferential alignment of the fibrin fibrils induced by compaction of the shell relative to the core and that any effect of the interface between the core and the shell associated with the fabrication procedure did not grossly affect the cell behavior.

Less Circumferential RDF Alignment Occurs in Floating Core Stimulus FPCMs, and Radial Alignment Occurs in Embedded Core Stimulus FPCMs

Having established the validity and performance of the FPCM assay by characterizing the case of a FPCM without PECs in the core, we investigated the more complex case of a FPCM with PECs in the core. The

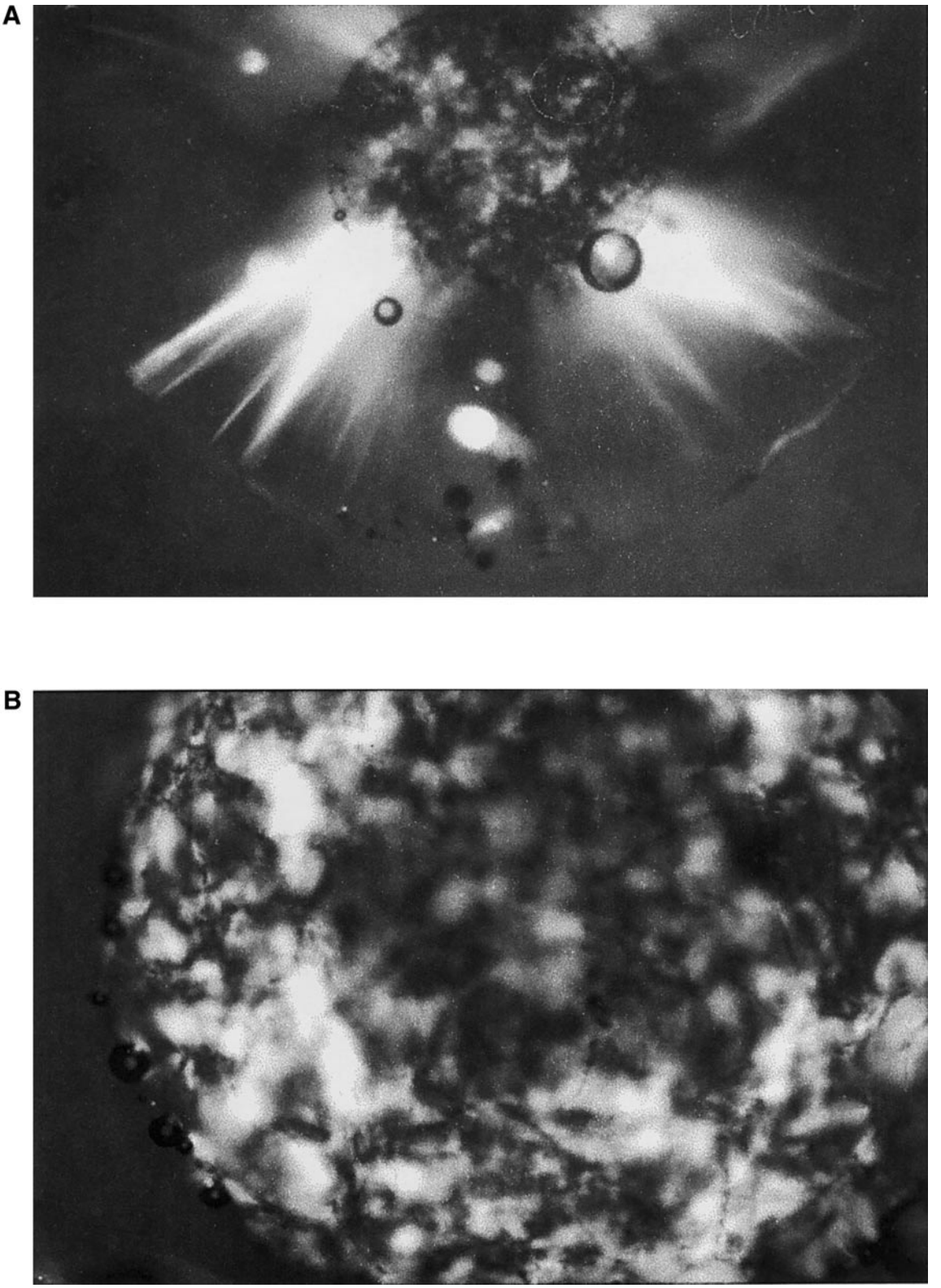

FIG. 8. Polarized light micrographs of (A) Inverse and (B) Base FPCMs. Bright regions due to birefringence occur wherever fibril alignment was not coaligned with either the vertically aligned polarizer or the horizontally aligned analyzer, with maximal brightness occurring where the direction of fibril alignment was offset 45° ("diagonal") with respect to the crossed polarizing filters. (The entirety of the FPCMs could not be captured in a single photograph because of their size.) In the Inverse case (A), the crossed polars are easily seen as

TABLE 2

FPCMs with PECs in the Core (Core Stimulus FPCMs)

PEC (cells/ml)	n	$<\chi>_{free}$	$<\chi>_{embed}$	Time (h)	$<\rho_{shell}>$ (%)	$<\Phi>_{free}$	σ_Φ	$<\Phi>_{embed}$	σ_Φ
1.0×10^5	6	0.77	0.76	24	12	0.46	0.04	0.49	0.02
				48	39	0.33	0.07	0.54	0.02
1.0×10^6	6	0.66	0.71	24	10	0.46	0.03	0.61	0.01
				48	34	0.45	0.02	0.59	0.02
5.0×10^6	6	0.70	0.73	24	9	0.48	0.01	0.61	0.02
				48	24	0.44	0.01	0.60	0.02
1.0×10^7	6	0.71	0.74	24	8	0.52	0.03	0.74	0.02
				48	22	0.49	0.03	0.71	0.02

Note. σ_Φ denotes standard error of the mean.

supposition was that the PECs would release one or more chemotactic factors in the core, which would diffuse radially outward through the shell and thereby affect the RDF alignment. It was presumed that the fibroblasts with radial alignment were actually oriented toward the core due to positive chemotaxis. Assuming the RDFs were not completely inhibited from compacting the shell of floating FPCMs by diffusible PEC factors, a radial chemotactic cue would then be competing with the circumferential contact guidance cue.

Figure 7D suggests that the alignment of RDFs in a FPCM with PECs in the core was clearly different from the corresponding case without PECs in the core (compare to Fig. 7A). As a control, we loaded FPCM cores with 10-μm latex beads at a volume fraction similar to that of the PECs in Core stimulus FPCMs (ca. 1% v/v); values of $<\Phi>_n$ were similar to those of Base FPCMs (not shown), suggesting that chemotactic gradients emanating from the PECs are the cause of the altered fibroblast alignment. Note that the presence of PECs caused the FPCMs to compact more slowly. However, even when the degree of FPCM compaction, as measured by ρ_{shell}, and, hence, the strength of fibrin fibril alignment were similar to those obtained for FPCMs without PECs in their cores, strong circumferential cell alignment did not occur (compare $<\Phi>_n$ values for cases in Table 2, where ρ_{shell} is similar to the Base case of Table 1). A two-way ANOVA demonstrated that RDF alignment depended on both the concentration of PECs in the core ($P = 0.03$) and the incubation time ($P = 0.04$), as seen in Fig. 9. The interaction of PEC concentration and incubation time was not significant ($P = 0.33$). The value of $<\Phi>_n$ increased with higher PEC concentrations and decreased with longer incubation time. These results are consistent with a steeper gradient of a chemotactic factor(s) being generated by an increased number of PECs in the core and a strengthening circumferential contact guidance field as compaction proceeds with time. In further support of this explanation, a similar dose–response experiment was conducted, comparing floating and embedded Core stimulus FPCMs. As expected, abolishing compaction and associated circumferential contact guidance in the embedded FPCMs resulted in a dominant chemotactic response manifested by radial alignment (Fig. 9). The alignment of the fibroblasts was dependent on the PEC concentration ($P < 0.001$), but not the incubation time ($P = 0.92$).

DISCUSSION

We have described a novel *in vitro* assay conceived to facilitate systematic study of the interplay among fibroblast behavior, chemotactic factors, and tissue mechanics leading to contact guidance. Our assay is distinguished by the ability to generate predictable diffusion gradients of chemotactic factors in the fibrin gel and the dependence of variables on only a single (radial) coordinate, which is not the case for the more obvious cylindrical geometry. While the use of PECs in the studies reported here inherently precludes predictable diffusion gradients, we have also employed controlled release polymer beads encapsulating the peptide GRGDSP [24], which we have shown to be chemotactic [25]. The advantage of a predictable diffu-

perpendicular black bands (extinction regions) across the FPM in the horizontal and vertical directions, separating four birefringent regions with "diagonal" alignment in the shell associated with radially aligned fibrils. In the Base case (B), the presence of cells in the shell interferes with the birefringence, but four birefringent regions consistent with circumferential fibril alignment are still discernible in the shell; birefringent regions again occurred due to "diagonal" alignment, because circumferentially aligned fibrils in those regions were not coaligned with either the analyzer or the polarizer. Birefringent regions were not observed in either FPMs or Control FPCMs (not shown).

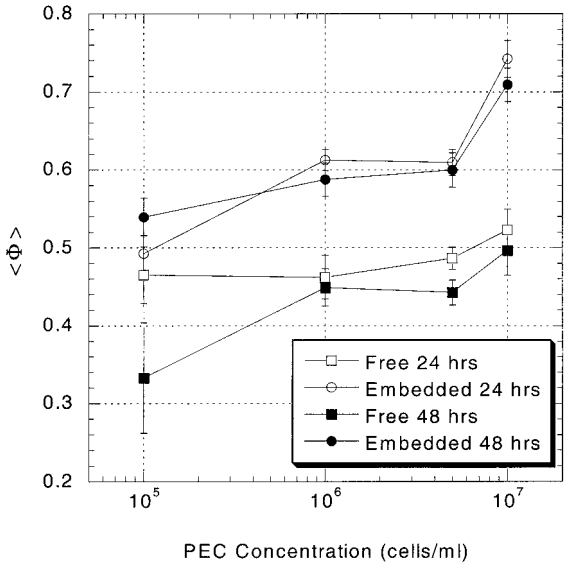

FIG. 9. Dose–response plot of RDF alignment to PEC concentration comparing free-floating and Embedded FPCMs after 24- and 48-h incubations. For floating FPCMs, $<\Phi>$ increases with increasing PEC concentration in the core, which is consistent with chemotactic factors being released by the PECs (two-way ANOVA, $P = 0.03$). RDF alignment becomes more circumferential with time as the FPCM compacts and the circumferential contact guidance field strengthens ($P = 0.04$). This also may reflect the chemotactic factor gradient generated by PECs, becoming shallower and/or associated with suboptimal concentrations. At the highest PEC loading, the circumferential contact guidance field and the radial chemotactic stimulus apparently negate each other to yield random orientation ($<\Phi> \sim 0.5$). For Embedded FPCMs, $<\Phi>$ increases above the isotropic value of 0.5 with increasing PEC concentration in the core as the RDFs bias their orientation radially in response to the putative radial chemotactic stimulus (two-way ANOVA, $P < 0.001$). The alignment does not become more circumferential over time because there is no compaction-induced circumferential contact guidance field ($P = 0.92$).

sion gradient depends on the ability to fabricate an FPCM with sufficient approximation of spherical symmetry. While we have determined limits of core-shell eccentricity that appear consistent with this approximation in practice, it is also important to note that other factors such as significant spatial variations in initial fibroblast concentration may invalidate the assumption of spherical symmetry even if the FPCMs are concentric. The main cause, cell settling during FPCM fabrication, can be readily minimized when using fibrin gel because of the relatively rapid fibrillogenesis that can be attained by adjusting the thrombin concentration which entraps the cells before settling can occur.

We have explained how the interplay of circumferential contact guidance generated by FPCM compaction and radial chemotaxis due to factors released in the core by the PECs results in the observed RDF alignment. Our theoretical explanation that RDFs in the shell caused compaction of the shell relative to the core and consequent alignment of the fibrin fibrils around the circumference, which dominated RDF alignment in the absence of a diffusible stimulus emanating from the core, was supported by the birefringence pattern in the Base FPCMs (Fig. 8B). A similar theoretical explanation for the radial contact guidance field in the Inverse FPCMs, which we investigated for assay validation purposes, was also supported by the birefringence pattern (Fig. 8A). The loss of circumferential cell alignment when loading the core with PECs, despite compaction and occurrence of a circumferential contact guidance field, is explainable by competition from a radially directed diffusion gradient of a chemotactic factor(s) released by the PECs. The inhibition of compaction observed at higher PEC loadings gives an additional advantage of the radial chemotactic gradient(s) over the circumferential contact guidance field which results from compaction of the shell relative to the core. The use of the Embedded FPCM, which abolished compaction and the circumferential contact guidance field, yielded the expected increase in radial alignment due to a pure chemotactic gradient(s). It has been reported that a factor secreted by macrophages inhibits collagen gel compaction by fibroblasts [26] and there are many reports of various chemotactic factors secreted by macrophages (reviewed in [27]), consistent with our observations.

The time scale for RDF population of the core via invasion and division was much longer than that for extensive compaction with our current experimental conditions. These time scales would have to be further equalized to simulate fibroplasia that precedes wound contraction if these types of studies are to simulate dermal wound healing. There are numerous ways of potentially accomplishing this, such as use of a potent migration stimulating factor or altering the fibrin network so as to promote migration and/or slow the rate of compaction, e.g., by crosslinking the fibrin with Factor XIII [28, 29].

Differences in fibroblast metabolism, phenotype, traction, and migration between floating (stress-free) and adherent (stressed) gels have been documented [30–32]. While it appears counterintuitive, the FPCM is not stress-free, even when floating (it clearly is not when embedded), because the acellular core effectively provides a mechanical constraint to compaction occurring in the shell, albeit a compliant one. This is more obvious if one considers the extreme case in which the core is formed from a rigid material rather than fibrin gel. In contrast, the FPM is essentially stress-free when floating; the finite permeability of the fibrin network causes it to develop stress as the interstitial medium flows out during compaction, but this stress is insignificant with FPMs of millimeter diameter [33].

We have elected to use a fibrin gel for our physiologically relevant experimental ECM because its rapid gelation helps ensure a uniform cell distribution and

its facile adhesivity helps ensure structural continuity between the core and the shell. Further, we have already characterized the mechanical properties of fibrin gel (unpublished data), thereby facilitating modeling with our theory for cell–matrix mechanical interactions. However, it is well known that wound contraction takes place within granulation tissue, a mixture of collagen, fibrin, fibronectin, and other matrix proteins [27]. Since the biochemistry of the ECM is known to modulate cellular behavior [27, 34, 35], the use of a purely fibrin gel undermines the physiological relevance of our results.

There are other variations of the FPCM assay that we plan to investigate. For example, the shell could be collagen gel instead of fibrin gel to more realistically represent the dermis, although sufficient adhesion of the two gels must be considered. The assay could be conducted for incubation times much longer than the limit imposed by loss of optical transparency (due to gel compaction) needed for light microscopy. Since the FPCM is essentially a coculture system, interactions between any two cell types can be readily studied in a physiologically relevant gel environment with or without a controlled release diffusion gradient emanating from the core.

This work has been supported by NIH P01-GM50150-03S1 (R.T.T.). Drs. Terrence Ryan, George Cherry, and David Knighton are gratefully acknowledged for the use of laboratory facilities as are Vance Fiegel, Amy Tranquillo, Matt McCoy, Jim Pray, Tim Johnson, and Cheryl Wotus for technical advice and assistance during the early phases of this project. The technical advice and assistance of Jeff Shearer, Ray Sicard, and Cindy Coulter are also gratefully acknowledged as is the assistance Allison Bain with statistical testing.

REFERENCES

1. Dvorak, H. F. (1986). Tumors: Wounds that do not heal. Similarities between tumor stroma generation and wound healing. *N. Engl. J. Med.* **315,** 1650–1659.
2. Stopak, D., and Harris, A. K. (1982). Connective tissue morphogenesis by fibroblast traction. I. Tissue culture observations. *Dev. Biol.* **90,** 383–398.
3. Grabel, L. B., and Watts, T. D. (1987). The role of extracellular matrix in the migration and differentiation of parietal endoderm from teratocarcinoma embryoid bodies. *J. Cell Biol.* **105,** 441–448.
4. Greiling, D., and Clark, R. A. (1997). Fibronectin provides a conduit for fibroblast transmigration from collagenous stroma into fibrin clot provisional matrix. *J. Cell Sci.* **110,** 861–870.
5. Oster, G. F., Murray, J. D., and Harris, A. K. (1983). Mechanical aspects of mesenchymal morphogenesis. *J. Embryol. Exp. Morphol.* **78,** 83–125.
6. Barocas, V. H., and Tranquillo, R. T. (1997). An anisotropic biphasic theory of tissue-equivalent mechanics: The interplay among cell traction, fibrillar network deformation, fibril alignment, and cell contact guidance. *J. Biomech. Eng.* **119,** 137–145.
7. Zicha, D., Dunn, G. A., and Brown, A. F. (1991). A new direct-viewing chemotaxis chamber. *J. Cell Sci.* **99,** 769–775.
8. Boyden, S. (1962). The chemotactic effect of mixtures of antibody and antigen on polymorphonuclear leucocytes. *J. Exp. Med.* **115,** 453–466.
9. Curtis, A. S., and Wilkinson, C. D. (1998). Reactions of cells to topography. *J. Biomater. Sci. Polym. Ed.* **9,** 1313–1329.
10. Walboomers, X. F., Ginsel, L. A., and Jansen, J. A. (2000). Early spreading events of fibroblasts on microgrooved substrates. *J. Biomed. Mater. Res.* **51,** 529–534.
11. Dunn, G. A., and Brown, A. F. (1986). Alignment of fibroblasts on grooved surfaces described by a simple geometric transformation. *J. Cell Sci.* **83,** 313–340.
12. Bell, E., Ivarsson, B., and Merrill, C. (1979). Production of a tissue-like structure by contraction of collagen lattices by human fibroblasts of different proliferative potential *in vitro. Proc. Natl. Acad. Sci. USA* **76,** 1274–1278.
13. Tuan, T. L., Song, A., Chang, S., Younai, S., and Nimni, M. E. (1996). In vitro fibroplasia: Matrix contraction, cell growth, and collagen production of fibroblasts cultured in fibrin gels. *Exp. Cell Res.* **223,** 127–134.
14. Mochitate, K., Pawelek, P., and Grinnell, F. (1991). Stress relaxation of contracted collagen gels: Disruption of actin filament bundles, release of cell surface fibronectin, and down-regulation of DNA and protein synthesis. *Exp. Cell Res.* **193,** 198–207.
15. Grinnell, F., and Lamke, C. R. (1984). Reorganization of hydrated collagen lattices by human skin fibroblasts. *J. Cell Sci.* **66,** 51–63.
16. Lorimier, S., Hornebeck, W., Godeau, G., Pellat, B., Gillery, P., Maquart, F. X., and Laurent-Maquin, D. (1998). Morphometric studies of collagen and fibrin lattices contracted by human gingival fibroblasts: Comparison with dermal fibroblasts. *J. Dent. Res.* **77,** 1717–1729.
17. Moon, A. G., and Tranquillo, R. T. (1993). The fibroblast-populated collagen microsphere assay of cell traction force. Part 1. Continuum model. *AIChE J.* **39,** 163–177.
18. Barocas, V. H., Moon, A. G., and Tranquillo, R. T. (1995). The fibroblast-populated collagen microsphere assay of cell traction force. Part 2. Measurement of the cell traction parameter. *J. Biomech. Eng.* **117,** 161–170.
19. Freshney, R. I. (1987). "Culture of Animal Cells: A Manual of Basic Technique," 2nd ed., A. R. Liss, New York.
20. Shearer, J. D., Richards, J. R., Mills, C. D., and Caldwell, M. D. (1997). Differential regulation of macrophage arginine metabolism: A proposed role in wound healing. *Am. J. Physiol.* **272,** E181–190.
21. Tsunawaki, S., Sporn, M., Ding, A., and Nathan, C. (1988). Deactivation of macrophages by transforming growth factor-beta. *Nature* **334,** 260–262.
22. Wahl, S. M. (1992). Transforming growth factor beta (TGF-beta) in inflammation: A cause and a cure. *J. Clin. Immunol.* **12,** 61–74.
23. Shearer, J. D., Aberle, L. A., Richards, J. R., and Caldwell, M. D. (1995). Flow cytometric analysis of wound cell replication. *Wound Repair Regen.* **3,** 104.
24. Bromberek, B. A., Knapp, D. M., Enever, P. A. J., Caldwell, M. D., and Tranquillo, R. T. (2001). The fibroblast-populated microsphere wound healing assay: Use of controlled release of GRGDSP to elicit chemotaxis. In preparation.
25. Knapp, D. M., Helou, E. F., and Tranquillo, R. T. (1999). A fibrin and collagen gel assay for tissue cell chemotaxis: Assessment of fibroblast chemotaxis to GRGDSP. *Exp. Cell Res.* **247,** 543–553, doi: 10.1006/excr.1998.4364.
26. Ehrlich, H. P., and Rajaratnam, J. B. (1990). Cell locomotion forces versus cell contraction forces for collagen lattice contrac-

tion: An in vitro model of wound contraction. *Tissue Cell* **22,** 407–417.

27. Clark, R. A. F. (1996). Wound repair: Overview and general considerations. *In* "The Molecular and Cellular Biology of Wound Repair" (R. A. F. Clark, Ed.), Plenum, New York.
28. Brown, L. F., Lanir, N., McDonagh, J., Tognazzi, K., Dvorak, A. M., and Dvorak, H. F. (1993). Fibroblast migration in fibrin gel matrices. *Am. J. Pathol.* **142,** 273–283.
29. Guyton, A. C. (1991). "Textbook of Medical Physiology," 8th ed., Saunders, Philadelphia.
30. Grinnell, F. (1994). Fibroblasts, myofibroblasts, and wound contraction. *J. Cell Biol.* **124,** 401–404.
31. Knapp, D. M., Tower, T. T., and Tranquillo, R. T. (1999). Estimation of cell traction and migration in an isometric cell traction assay. *AIChE J.* **45,** 2628–2640.
32. Shreiber, D. I., Enever, P. A. J., and Tranquillo, R. T. (2001). Effects of PDGF-BB on rat dermal fibroblast behavior in mechanically stressed and unstressed collagen and fibrin gels. *Exp. Cell Res.* **266,** 155–166, doi: 10.1006/excr.2001.5208.
33. Barocas, V. H., and Tranquillo, R. T. (1994). Biphasic theory and *in vitro* assays of cell-fibril mechanical interactions in tissue-equivalent collagen gels. *In* "Cell Mechanics and Cellular Engineering" (V. C. Mow, F. Guilak, R. Tran-Son-Tay, and R. M. Hochmuth, Eds.), Springer-Verlag, New York.
34. Ware, M. F., Wells, A., and Lauffenburger, D. A. (1998). Epidermal growth factor alters fibroblast migration speed and directional persistence reciprocally and in a matrix-dependent manner. *J. Cell Sci.* **111,** 2423–2432.
35. Maheshwari, G., Wells, A., Griffith, L. G., and Lauffenburger, D. A. (1999). Biophysical integration of effects of epidermal growth factor and fibronectin on fibroblast migration. *Biophys. J.* **76,** 2814–2823.

Received July 31, 2001
Revised version received December 31, 2001
Published online March 26, 2002